

Lattice approach to the dynamics of phase-coded soliton trains

This article has been downloaded from IOPscience. Please scroll down to see the full text article.

2012 J. Phys. A: Math. Theor. 45 025202

(<http://iopscience.iop.org/1751-8121/45/2/025202>)

View [the table of contents for this issue](#), or go to the [journal homepage](#) for more

Download details:

IP Address: 134.151.33.144

The article was downloaded on 14/12/2011 at 12:39

Please note that [terms and conditions apply](#).

Lattice approach to the dynamics of phase-coded soliton trains

Jaroslav E Prilepsky¹, Stanislav A Derevyanko¹ and Sergei K Turitsyn²

¹ Nonlinearity and Complexity Research Group, Aston University, Birmingham B4 7ET, UK

² Photonics Research Group, Aston University, Birmingham B4 7ET, UK

E-mail: y.prylepskiy1@aston.ac.uk

Received 11 August 2011, in final form 25 October 2011

Published 8 December 2011

Online at stacks.iop.org/JPhysA/45/025202

Abstract

We address the collective dynamics of a soliton train propagating in a medium described by the nonlinear Schrödinger equation. Our approach uses the reduction of train dynamics to the discrete complex Toda chain (CTC) model for the evolution of parameters for each train constituent: such a simplification allows one to carry out an approximate analysis of the dynamics of positions and phases of individual interacting pulses. Here, we employ the CTC model to the problem which has relevance to the field of fibre optics communications where each binary digit of transmitted information is encoded via the phase difference between the two adjacent solitons. Our goal is to elucidate different scenarios of the train distortions and the subsequent information garbling caused solely by the intersoliton interactions. First, we examine how the structure of a given phase pattern affects the initial stage of the train dynamics and explain the general mechanisms for the appearance of unstable collective soliton modes. Then we further discuss the nonlinear regime concentrating on the dependence of the Lax scattering matrix on the input phase distribution; this allows one to classify typical features of the train evolution and determine the distance where the soliton escapes from its slot. In both cases, we demonstrate deep mathematical analogies with the classical theory of crystal lattice dynamics.

PACS numbers: 05.45.Yv, 42.81.Dp, 45.05.+x, 02.10.Yn

(Some figures may appear in colour only in the online journal)

1. Introduction

The nonlinear Schrödinger equation (NLSE) represents one of the most ubiquitous physical models occurring when the effects of weak nonlinearity compete with the dispersion of a narrow field envelope [1]. This equation is integrable by the inverse scattering transform method [1, 2] and admits highly robust soliton solutions, which can propagate through the

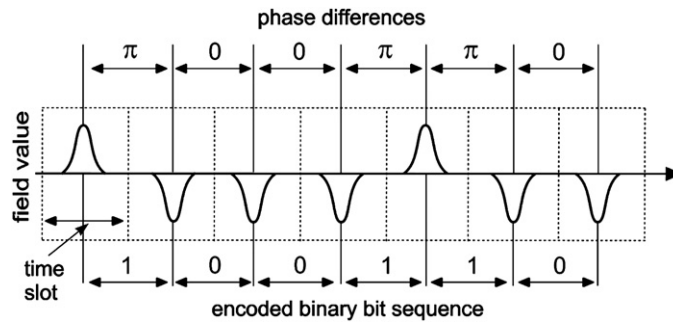


Figure 1. Example of the RZ-DPSK encoded train referring to {1 0 0 1 1 0} sequence of bits.

media without shape distortion. It is this property of the solitons which makes them good candidates for the transmission of information in optical fibres (at least in low bit rate regimes $< 10 \text{ Gb s}^{-1}$ which is the present-day standard) [3].

Solitons can be used in a highly popular way of encoding an informational stream frequently implemented in modern lightwave (optical) transmission lines which utilizes the phase modulation of the carrying wave [4–6]. For the binary digital coding one can ascribe the logical ‘unities’ to be encoded onto a π phase change between the adjacent pulses, whereas logical ‘zeros’ to correspond to a zero phase shift. In the theory of information transmission such a binary phase encoding is called the *differential phase-shift-keying format*, and we will use the conventional abbreviation DPSK below to name our encoding scheme. In particular, in the return-to-zero (RZ) DPSK format the information is encoded by the phase difference between the two adjacent *well-separated localized pulses* [5, 6]: the key idea of this RZ DPSK format is illustrated in figure 1.

For a fibre optical transmission channel, an arbitrary informational message can be encoded using the RZ DPSK format as a sequence of localized pulses with correspondingly chosen phase differences between the adjacent pulses (each taking values either 0 or π for the binary format, see figure 1). The high-quality error-free transmission corresponds to the ideal case when the pulses do not wander far from their initial positions staying inside their assigned slots and do not change their phase differences significantly. There exists a multitude of sources of signal distortion [4–7], and in this study, we will be concerned with one of them: the information garbling caused by the *intrachannel pulse interactions* of separated pulses. Such effects arise due to the mutual (relatively weak) overlap of the tails of pulses belonging to adjacent slots: after a long propagation distance some of them will move far away from initial positions and collide (or either drift off from the rest for a finite train). The phase differences are also altering during the train propagation. In this paper, we propose a mathematical concept for analysing how the initial distribution of bits (i.e. a given particular set of binary phases) affects the dynamics of the whole pattern, in particular, the rates at which pulses converge to/diverge from each other.

Clearly, the direct numerical modelling of large pulse trains has only a limited merit. Firstly, it does not tell us much about the distortion rate for large sequences, and for each new sequence one would have to run the simulation from scratch. Secondly, the number of possible patterns grows as 2^N , where N is the size of the pattern, and already for a relatively small number of bits the computational time can become forbiddingly large. This is one of the reasons why in practice only very short patterns are usually considered, while in the information theory, one commonly operates with patterns as long as a few millions. However when pulses are

localized and well separated, it is often possible to reduce the description from a system with distributed parameters (like NLSE) to a simplified system of ODEs, i.e. a finite-dimensional system: the latter describes the evolution of some particular parameters of individual pulses. Such a simplified approach is often called the collective coordinate method [8]. In the case of NLSE channel, the fundamental soliton solutions serve as phase-coded localized pulses used for the transmission. For the particular choice of the soliton transmission format (i.e. for NLSE solitons), this reduction to the collective coordinates can be proven to be asymptotically exact: it can be done by means of the machinery of adiabatic soliton perturbation theory [9]. Then under some additional assumptions imposed on the model parameters, these ODEs can be further reduced to the integrable complex Toda chain (CTC) model [10–13] (see also papers [14, 15]): the relevant details are briefly summarized in section 2. One can therefore hope that the insight obtained in this paper by looking into the specific choice of soliton transmission format can be helpful for considering the properties of arbitrary RZ-DPSK formats.

The effects of inter-soliton interaction eventually lead to the appearance of errors in the bit stream. Let us note that although this study is driven primarily by the applications in fibre optical communications, the mathematical approach used in the paper is rather generic and valid for the description of a broad spectrum of physical problems referring to the complexes of interacting solitons like e.g. the soliton trains of the modified NLSE [16] or the discrete Ablowitz–Ladik chain [17]. Possible applications may also involve soliton (matter wave) chains in the Bose–Einstein condensate [18], massive Thirring model [19] and to some extent the multicomponent NLSE generalizations [20]. The underlying idea of the current work is the application of the methods known from the theory of crystal lattice vibrations [21] (and more generally, matrix perturbation theory [22, 23]) to studying the collective motion (modes) of the interacting soliton train. The individual solitons then play the role of effective particles coupled either elastically or nonelastically to the nearest neighbours via the tails of their field distribution.

For the purposes of pattern transmission, it is often sufficient to consider only the initial stage of the soliton train evolution, since at long distances the information gets completely distorted by the interaction-induced pulse walk-off. Then it is sufficient to linearize the aforementioned effective system of ODEs around the initial configuration which is, in turn, determined by the input bit pattern. After the linearization, one ends up with a set of linear differential–difference equations which are very similar to those of the theory of crystal lattice dynamics. We address the general structure of these linearized equations and their solutions in section 3. Analysing the eigenvalues of the emerging linear self-adjoint eigenproblem, one can determine directly the properties of collective modes for the soliton lattice, (see also the preliminary analysis of the problem in [24]). The eigenmode with the highest growth increment can be used as an estimate for the overall rate of the train distortion and, hence for the evaluation of the maximum error-free propagation distance. Note that the linearization of the CTC model was already considered in [14], where, however, another source of the system excitation (in-line noise) was studied. In section 3.2, we deal with the homogeneous (marginal) input bit distributions, i.e. consider the patterns consisting of either pure ‘zeros’ or ‘unities’. For the former all nontrivial modes are unstable, while the latter case, alternatively, appears to be linearly stable: in this sense these cases are the marginal scenarios for arbitrary intermediate input bit patterns. The local deviations from the uniform pattern are considered in section 4. There is a nice mathematical analogy between the instabilities induced by the non-homogeneity of the pattern (i.e. the appearance of ‘zeros’ in the stream of pure ‘unities’) and the appearance of localized defect modes in a nonuniform crystal lattice [21]. First, we recall some pertinent elements of the matrix perturbation theory to obtain the expression for the Green function of the inhomogeneous system, see section 4.1. Then in section 4.2, we

apply this tool for finding the eigenvalues, instability increments and localization lengths of the inhomogeneous patterns, and in section 4.4 provide some notes on generic bit patterns. In section 5, we consider the case of a nonlinear dynamical regime for CTC and address the properties of the Lax scattering matrix for the integrable CTC. By means of the non-Hermitian generalization of the approach from sections 3 and 4, it is possible to study the eigenvalue properties of the Lax matrix versus the input bit pattern. We utilize the form of the eigenvalue distribution to classify the ensuing patterns [13] and provide some estimates for the length scale of pattern corruption in dependence on the input sequence. Finally, in section 6, we perform numerical simulations and present some direct applications of the results obtained referring to characteristic distortion scales in dependence on the input phase distribution. The findings are then summarized in the conclusion.

2. The model and problem statement

In this section, we briefly recall the necessary conditions for the CTC-model validity for a NLSE soliton train [10–12], and then apply it specifically to the DPSK encoding format. As mentioned in the introduction, the analogous treatment of soliton trains in other nonlinear integrable models is possible as well [16].

The NLSE with constant anomalous dispersion written in dimensionless soliton units reads as

$$\frac{\partial Q}{\partial z} - \frac{i}{2} \frac{\partial^2 Q}{\partial t^2} - i|Q|^2 Q = 0. \quad (1)$$

Since we have the fibre optics applications in mind, the independent variable z (coordinate along the length of the fibre) plays the role of time variable, and the variable t plays the role of ‘space’ coordinate [3]. Naturally one can easily recast the results of this paper to conventional NLSE notations (with the reversed meaning of independent variables) used in other applications.

We deal with the input having the form of the sum (train) of separated fundamental NLSE solitons:

$$Q(t; 0) = \sum_{n=0}^N \frac{2v_n e^{i\phi_n(t)}}{\cosh[2v_n(t - \xi_n)]}, \quad (2)$$

where

$$\phi_n(t) = 2\mu_n(t - \xi_n) + \delta_n,$$

and δ_n , ξ_n , $2v_n$ and $2\mu_n$ are the phase, position, amplitude and frequency (velocity) of the n th individual soliton from the train, respectively, with $N + 1$ being the total number of solitons in the train. The weak exponential overlap between the adjacent solitons, $\exp[-v_n(\xi_{n+1} - \xi_n)]$, is supposed to be the small parameter of the problem, i.e. the solitons are well separated.

For our task, we assume that the initial amplitudes and velocities of the individual solitons are identical: $v_n^0 \equiv v$, $\mu_n^0 \equiv \mu$. Then for simplicity we will work in the reference frame attached to the train and set $\mu = 0$. After that, we introduce the complex quantity q_n as

$$q_n = -2v\xi_n(z) + 2n \ln 2v + i[n\pi - \delta_n(z)], \quad (3)$$

which involves the individual soliton position, ξ_n , and phase, δ_n . The z -dependences of the soliton phase and position for the case of a single unperturbed soliton have the form

$$\delta_n(z) = 2 \int_0^z v_n^2 dz' + \delta_n^0, \quad \xi_n(z) = \xi_n^0, \quad (4)$$

where δ_n^0 and ξ_n^0 are the corresponding initial values (soliton velocity is set to zero). So one has a ‘fast’ homogeneous rotation of the phase due to the self-phase modulation (the term $\sim v^2 z$), which is, however, irrelevant for the DPSK encoding since we operate with the relative phase differences only (at least when the amplitude distortion can be neglected). The increment between the two adjacent pulses is given by

$$q_{n+1} - q_n = -2v(\xi_{n+1} - \xi_n) + 2 \ln 2v + i[\pi - (\delta_{n+1} - \delta_n)]. \quad (5)$$

The information encoded into the n th bit enters via the phase difference: $\delta_{n+1} - \delta_n$.

The simplified dynamics of the train can be described by means of the integrable CTC (see [10–12, 16] for additional details):

$$\frac{d^2 q_n}{dz^2} = e^{q_{n+1} - q_n} - e^{q_n - q_{n-1}}, \quad n = 0, \dots, N, \quad (6)$$

where we have applied the renormalization: $4vz \rightarrow z$. The conditions for the applicability of the CTC (6) match the requirements imposed by the transmission needs. First, the relative deviation of velocities and amplitudes of individual solitons in the input form (2) must be small (these are actually set to zero in our analysis). Secondly, the solitons must be well separated and distinguishable, and hence the aforementioned parameter $\exp[-v_n(\xi_{n+1} - \xi_n)]$ involving the soliton amplitude v and the intersoliton separation, $\xi_{n+1} - \xi_n$ is small as well. Then the dynamics of soliton positions and phases can be described by the CTC (6) with a good accuracy [10–12, 16]. We will assume the finiteness of the train, so that in equation (6) the subindex counting the solitons, n , runs from 0 to N . Since there are no solitons with numbers $n = -1$ and $n = N + 1$, the following boundary conditions are imposed: $\exp(-q_{-1}) = \exp(q_{N+1}) \equiv 0$.

The dynamics of the complex variables q_n provides the information about the positions of individual solitons (via its real part) and their phases (via its imaginary part). Studying the evolution of q_n , one can describe the interaction-induced changes (so-called jitters) of the pulse position and phase that are the principal effects leading to the corruption of encoded information.

3. The initial stage of the instability: linear evolution of the DPSK-encoded pulse train

In this section, we are interested in the initial stages of propagation where the information is still not significantly corrupted, and therefore the dynamical properties can be analysed via the CTC system linearized around the initial input values of q_n . This approach is meaningful for studying the onset of instabilities: one can find the growth increments, symmetry and activation features of the unstable modes.

3.1. General structure of the linearized dynamical equations

Note that to encode N bits, we need N phase differences, i.e. $N + 1$ soliton pulses. We will assume here that initially all solitons are equidistant with the common distance $r = \xi_{n+1}^0 - \xi_n^0$ and have the same amplitude v .

To study the initial stage of the instability, we linearize the system (6) around the initial configuration (labelled with the superscript ‘0’):

$$q_n(z) = q_n^0 + w_n(z), \quad w_n \ll q_n^0. \quad (7)$$

Then the initial differences are

$$q_{n+1}^0 - q_n^0 = -2vr + 2 \ln 2v + i[\pi - \Delta_1 \delta_n], \quad n = 0, \dots, N - 1,$$

where we have introduced the first forward difference operator, $\Delta_1 \delta_n \equiv \delta_{n+1} - \delta_n$. It will also be convenient to designate different bit patterns as $\{\dots\}_N$, where the interior of the braces displays a particular bit sequence, and subscript identifies the total number of bits.

For an arbitrary DPSK-encoded input we have (i) $\Delta_1 \delta_n = 0$ for a ‘zero’ bit number $n + 1$ and (ii) $\Delta_1 \delta_n = \pi$ for a logical ‘unity’ at the same position. One can write this as $\Delta_1 \delta_n = \pi b_{n+1}$, where b_{n+1} is the transmitted bit value, $b_{n+1} = 0, 1$. We define the universal z -scale, $a = 2\nu \exp(-r\nu)$, and use it to rescale the distance again: the eventual scaling now is $4\nu az \rightarrow z$.

After the linearization of equation (6) with respect to $w_n(z)$, we arrive at the set of inhomogeneous equations, which we write in the form

$$\frac{d^2 \mathbf{w}}{dz^2} = \hat{\Lambda} \mathbf{w} + \mathbf{f}, \tag{8}$$

where the bold symbols stand for a vector notation and an additional hat indicates a matrix. The $(N + 1) \times (N + 1)$ matrix $\hat{\Lambda}$ is real, symmetric and tridiagonal. Its elements depend on the values b_n of transmitted bit pattern, $\{b_1, \dots, b_N\}_N$, as follows:

$$\hat{\Lambda} = \begin{pmatrix} -\sigma_1 & \sigma_1 & 0 & \dots & 0 & 0 & 0 \\ \sigma_1 & -(\sigma_1 + \sigma_2) & \sigma_2 & \dots & 0 & 0 & 0 \\ \dots & \dots & \dots & \dots & \dots & \dots & \dots \\ \dots & \dots & \dots & \dots & \dots & \dots & \dots \\ 0 & 0 & 0 & \dots & \sigma_{N-1} & -(\sigma_{N-1} + \sigma_N) & \sigma_N \\ 0 & 0 & 0 & \dots & 0 & \sigma_N & -\sigma_N \end{pmatrix}, \tag{9}$$

where we have introduced the bit indicator quantities σ_n as

$$\sigma_n = (-1)^{1+b_n}, \quad n = 1, \dots, N. \tag{10}$$

The driving vector \mathbf{f} (containing $N + 1$ elements) is

$$\mathbf{f} = [\sigma_1, \sigma_2 - \sigma_1, \sigma_3 - \sigma_2, \dots, \sigma_N - \sigma_{N-1}, -\sigma_N]^T. \tag{11}$$

The initial conditions (ICs) for equations (8) can be obtained by recalling equations (3) and (4) as follows:

$$\mathbf{w}(0) = 0, \quad \mathbf{w}'(0) = -2i \frac{\nu^2}{4\nu a} \mathbf{1} = -i\alpha \mathbf{1}. \tag{12}$$

Here, $\alpha = \exp(r\nu)/4$, and $\mathbf{1} = [1, 1, \dots, 1]^T$ is the vector of dimension $N + 1$ containing only unities. Because $\exp(-r\nu)$ is a small parameter, α is large, while in equations (8) all rescaled coefficients and the inhomogeneity term are of the order of unity.

Now one can find the set of normalized orthogonal (real) eigenvectors \mathbf{v}_k and corresponding eigenvalues λ_k of $\hat{\Lambda}$. The solution of the system (8) and (12) can be written as an eigenvector expansion:

$$\mathbf{w} = \sum_k U_k(z) \mathbf{v}_k.$$

The general solution of equations (8) and (12) is the sum of two partial ones,

$$\mathbf{w} = \mathbf{w}_i + \mathbf{w}_f = \sum_k [U_k^i(z) + U_k^f(z)] \mathbf{v}_k, \tag{13}$$

where \mathbf{w}_i satisfies the homogeneous reduction of equation (8) with inhomogeneous ICs (12), whereas \mathbf{w}_f satisfies the inhomogeneous equation (8) but with zero ICs. We start with the former. The equations and ICs for the coefficients $U_k(z)$ are

$$\begin{aligned} \frac{d^2 U_k^i(z)}{dz^2} &= \lambda_k U_k^i(z), \\ U_k^i(0) &= 0, \quad \frac{dU_k^i(0)}{dz} = \alpha_k, \end{aligned} \tag{14}$$

where α_k is the projection of the initial derivative onto the corresponding eigenvector: $\alpha_k = \mathbf{w}'(0) \cdot \mathbf{v}_k$. Introducing the notations $\gamma_k = \sqrt{|\lambda_k|}$, we can see that for the particular solution satisfying the initial condition only, we have

$$U_k^i(z) = \alpha_k u_k(z), \quad u_k(z) = \begin{cases} \gamma_k^{-1} \sin \gamma_k z & \text{for } \lambda_k < 0, \\ \gamma_k^{-1} \sinh \gamma_k z & \text{for } \lambda_k > 0, \\ z & \text{for } \lambda_k = 0. \end{cases} \quad (15)$$

For any bit pattern there always exists a zero eigenvalue corresponding to the uniform phase rotation, see equation (4), which can be easily compensated and will be discarded in what follows. In the theory of crystal lattice dynamics such a common uniform displacement of atoms is removed by imposing an additional constraint on \mathbf{w} .

The sum of the elements in each row of matrix $\hat{\Lambda}$ is zero. Therefore the sum of all elements of each of its nontrivial eigenvectors (corresponding to non-zero eigenvalues), \mathbf{v}_k , is zero as well. This means that the projections α_k of the initial conditions onto the nontrivial eigenvectors are always zero, i.e. the vector of ICs, equation (12), is orthogonal to these eigenvectors: $\alpha_k = 0$ for $k \neq 0$. Hence, the ICs (12) can only excite a uniform phase drift of the soliton train mentioned above.

Now we turn to the particular solution of the inhomogeneous problem. Introducing the projections $f_k = \mathbf{f} \cdot \mathbf{v}_k$, we obtain the equation defining the functions $U_k^f(z)$:

$$\begin{aligned} \frac{d^2 U_k^f(z)}{dz^2} &= \lambda_k U_k^f(z) + f_k, \\ U_k^f(0) &= 0, \quad \frac{dU_k^f(0)}{dz} = 0. \end{aligned} \quad (16)$$

Its solution is

$$U_k^f(z) = f_k \int_0^z u_k(z - \tau) d\tau, \quad (17)$$

with u_k defined by (15).

For the subsequent analysis, we will also need the Green function for the matrix $\hat{\Lambda}$ defined as

$$\hat{G}(\lambda) \equiv (\lambda \hat{I} - \hat{\Lambda})^{-1}. \quad (18)$$

Its matrix elements are given as

$$G_{mn'}(\lambda) = \sum_{k=0}^N \frac{v_k^n v_k^{n'}}{\lambda - \lambda_k}, \quad (19)$$

where v_k^n and $v_k^{n'}$ are the n th and n' th elements of the eigenvector v_k . The poles of the trace of the Green function define the spectrum of the system.

At the end of this section, it is pertinent to note that while the ICs (12) are complex, the driving vector (11) is, in contrast, purely real. This means that only the real part of the general solution (13) can be excited, and according to the definition of q_n , equation (3), during this initial stage we have only the change of soliton positions (timing jitters) and no phase alternations take place (except for the irrelevant homogeneous shift). So, the changes of the phase differences (phase jitters) are only excited indirectly via the nonlinear corrections from the initial CTC (6), or due to the deviation of the dynamics described by the simplified CTC model from the full dynamics of soliton train in the NLSE, equation (1).

3.2. Uniform patterns: (i) pure zeros, $\{0\}_N$, and (ii) pure unities, $\{1\}_N$

Let us consider two very specific types of bit patterns for which the complete analytical expressions can be obtained, namely the patterns consisting of only zeros $\{0\}_N$ and those consisting of only unities, $\{1\}_N$ (see also [14, 15]).

Case (i). For the configuration $\{0\}_N$, we have for the bit indicators: $\sigma_n = -1$ for each site, and equations (8) transform into

$$-\frac{d^2 w_n}{dz^2} = \Delta_2 w_n, \quad n = 1, \dots, N - 1, \quad (20)$$

where Δ_2 is the second difference (discrete Laplace operator), $\Delta_2 w_n = w_{n+1} + w_{n-1} - 2w_n$. The equations for the boundary sites 0 and N are

$$-\frac{d^2 w_0}{dz^2} = 1 + w_1 - w_0, \quad -\frac{d^2 w_N}{dz^2} = -1 + w_{N-1} - w_N. \quad (21)$$

Equations (20) correspond to the semi-discrete limit of an elliptic second-order PDE. The presence of the boundary brings about the appearance of a nonzero driving term in equations (21) even when the bit pattern is uniform. The homogeneous part of boundary equations (21) corresponds to the free boundary sites, so the translational mode with zero eigenvalue exists as described in the previous subsection.

The matrix $\hat{\Lambda}$ defined by equations (20) and homogeneous part of equations (21), has a simple form, characteristic for the dynamics of an atomic crystal lattice. One can readily find its normalized eigenvectors

$$v_k^n = \begin{cases} \sqrt{\frac{2}{N+1}} \cos[\rho_k(n+1/2)], & k = 1, \dots, N \\ \frac{1}{\sqrt{N+1}}, & k = 0 \end{cases} \quad (22)$$

and eigenvalues

$$\lambda_k = \gamma_k^2 = 2(1 - \cos \rho_k) \geq 0, \quad (23)$$

where $\rho_k = \pi k/(N+1)$. Even k correspond to spatially symmetric eigenvectors while odd k correspond to an antisymmetric distribution.

We see that all nontrivial eigenmodes of the pattern $\{0\}_N$ are unstable, with the largest growth exponent located near the boundary of the Brillouin zone:

$$\gamma_N = \sqrt{2 + 2 \cos \frac{\pi}{N+1}},$$

so that $\gamma_N \approx 2$ for $N \gg 1$.

Case (ii). For the pure logical ‘unities’, $\{1\}_N$, we have $\sigma_n = 1$, and this case is tantamount to altering the signs on the lhs of equations (20) and (21):

$$\frac{d^2 w_n}{dz^2} = \Delta_2 w_n, \quad (24)$$

$$\frac{d^2 w_0}{dz^2} = 1 + w_1 - w_0, \quad \frac{d^2 w_N}{dz^2} = -1 + w_{N-1} - w_N. \quad (25)$$

Now equation (24) is of hyperbolic type and coincides exactly with the system governing the phonon dynamics in a uniform 1D crystal lattice [21]. Since this case differs from the previous one only by the sign of the matrix $\hat{\Lambda}$, the eigenvalues now change their sign:

$$\lambda_k = -2(1 - \cos \rho_k) \leq 0, \quad (26)$$

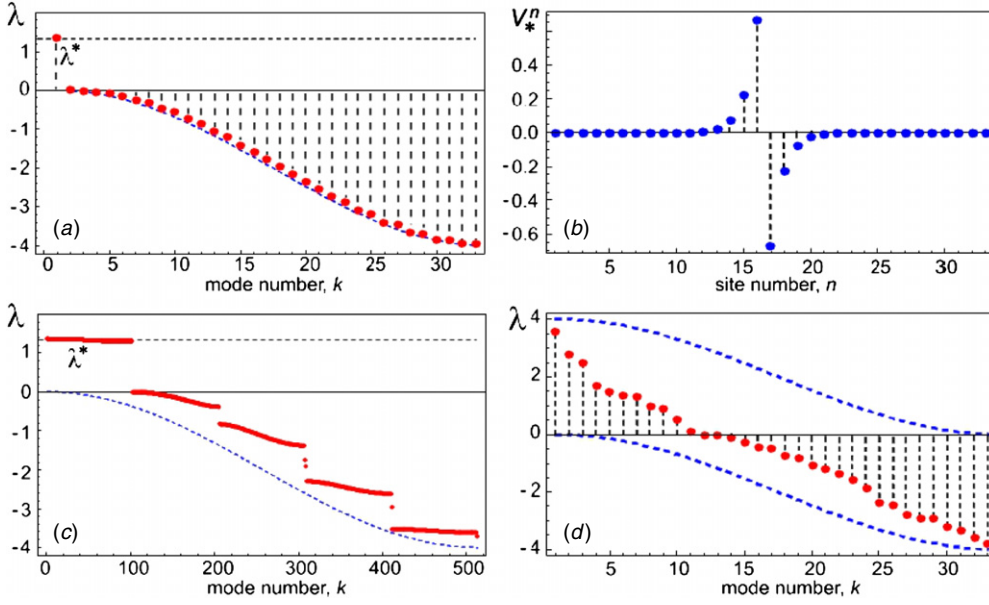


Figure 2. Eigenvalue distributions for several typical patterns. (a) The spectrum for the 32 bit pattern corresponding to a single ‘zero’ inside the uniform stream of ‘unities’; here we placed ‘zero’ at the position $s + 1 = 16$. The localized eigenvector for the unstable mode of the same pattern is plotted in the next panel (b). Panel (c) corresponds to the 512 bit pattern of ‘unities’ where every fifth bit was periodically replaced by a ‘zero’. The last panel (d) is a particular realization of the spectrum of a random 32 bit pattern (with equal probability to find either ‘zero’ or ‘unity’ at each position). The same realization is also considered in sections 5.4 and 6. In the panels (a), (c) and (d), the (blue) dashed lines correspond to the spectra of absolutely stable $\{1\}_{32}$ (below) and absolutely unstable $\{0\}_{32}$ (above) patterns, see equations (23) and (26).

while the eigenvectors remain the same, see equation (22). From (15), it follows that all nontrivial eigenmodes u_k are now non-growing oscillating functions. In the corresponding panels of figure 2, we depict the ‘marginal’ dependences (23) and (26) by the dashed lines. We note that a similar analysis of linear excitations for homogeneous CTC was carried out in [14] for a different source of driving and periodical boundary conditions. Our expressions for the spectral dependences (23), (26) and the eigenvectors (22) correspond to the Fourier series expansions of paper [14] in the limit of a large system.

For both uniform patterns $\{b\}_N$, where b is either ‘0’ or ‘1’, the projection of the driving term, \mathbf{f} , onto the eigenvectors of $\hat{\Lambda}$ is

$$f_k = \mathbf{f} \cdot \mathbf{v}_k = (-1)^{1+b} \frac{2\sqrt{2}}{\sqrt{N+1}} \sin \frac{\pi k}{2} \sin \frac{\pi k N}{2(N+1)}. \tag{27}$$

One can see that since the boundary forcing \mathbf{f} is antisymmetric, only antisymmetric modes with odd k are excited.

Finally, the Green function for both uniform patterns (we label it with the superscript ‘0’) is

$$G_{m'}^0(\lambda) = \frac{1}{N+1} \frac{1}{\lambda} + \frac{2}{N+1} \sum_{k=1}^N \frac{\cos[\rho_k(n+1/2)] \cos[\rho_k(n'+1/2)]}{\lambda - \lambda_k}. \tag{28}$$

We can simplify equation (28) by assuming that the number of bits, N , is large so one may use integration to evaluate the sum for, say, a stable pattern of ‘unities’ with the spectrum (26):

$$\begin{aligned} G_{mn'}^0(\lambda) &\approx \frac{2}{\pi} \int_0^\pi d\rho \frac{\cos[\rho(n+1/2)] \cos[\rho(n'+1/2)]}{\lambda + 2 - 2 \cos \rho} \\ &= \frac{1}{\sqrt{\lambda(4+\lambda)}} (F(\lambda)^{n+n'+1} + F(\lambda)^{|n-n'|}), \end{aligned} \quad (29)$$

where

$$F(\lambda) = \frac{\lambda + 2 - \sqrt{\lambda(4+\lambda)}}{2}, \quad (30)$$

and λ lies outside the spectral band $[-4, 0]$. In fact, the limit of equation (29) corresponds to a semi-infinite system, where the site positions n and n' are counted from the edge.

Let us now calculate the relative spreading for the stable pattern, $\{1\}_N$, at the initial stage of the evolution where $\gamma_k z \ll 1$. For such values of z from equation (17), we have $U_k^f(z) \sim z^2$, and $\mathbf{f}_k = (\delta_{0n} + \delta_{Nn})\mathbf{v}_k$. Due to the orthogonality of eigenvectors, the nonzero values of \mathbf{w} are

$$w_0(z) = -w_N(z) = z^2/2, \quad (31)$$

and the linear spreading of the boundary sites is $\xi_0(z) = \xi_0 - z^2/2$, $\xi_N(z) = \xi_N + z^2/2$ (in the renormalized units).

4. Nonuniform patterns and the onset of instability

In section 4.1, we recall some elements of the matrix perturbation analysis, which are subsequently applied to a single ‘zero’ bit incorporated into the stable pattern of ‘unities’ (sections 4.2 and 4.3). Section 4.4 deals with the general case.

4.1. Inverse matrix perturbation formula applied to the Green matrices

When performing the analysis of inhomogeneous cases, it is very convenient to utilize the formalism of matrix perturbation theory based on the Woodbury formula (WF) [23]. A somewhat simplified version of WF, which applies only to the case of single rank 1 perturbation, is often referred to as Sherman–Morrison formula, and a triple naming is also popular (for a thorough historical survey of the subject, applications and direct references see [22]).

The WF itself is introduced as follows. Suppose that a matrix \hat{A} is invertible. Let us now modify \hat{A} by introducing m rank 1 corrections (i.e. alter m of its rows or columns). In practice, the method is most effective when m is much smaller than the dimension (say N) of the original matrix, \hat{A} . After that we introduce two auxiliary rectangular matrices: the $N \times m$ matrix \hat{U} and the $m \times N$ matrix \hat{V} so that the product $\hat{U} \hat{V}$ has the same $N \times N$ dimension as the initial matrix \hat{A} . The next step is to recast the perturbation of our matrix \hat{A} (i.e. the difference between the original and altered matrices) in the form of the aforementioned product, $\hat{U} \hat{V}$; this decomposition is of course not unique and the particular choice of matrices \hat{U} and \hat{V} is just the matter of convenience. Then, if the $m \times m$ capacitance matrix, defined as

$$\hat{C} = \hat{I} - \hat{V} \hat{A}^{-1} \hat{U}, \quad (32)$$

is invertible, the inverse of the perturbed matrix can be embodied in the form given by the exact WF [22]:

$$(\hat{A} - \hat{U} \hat{V})^{-1} = \hat{A}^{-1} + \hat{A}^{-1} \hat{U} \hat{C}^{-1} \hat{V} \hat{A}^{-1}. \quad (33)$$

Turning to our problem, let our initial matrix be \hat{A}^0 of the form (9) and suppose that we know its spectrum. Then we seek for the spectrum of the perturbed one, $\hat{A} = \hat{A}^0 + \hat{U} \hat{V}$, where

m columns (rows) are different from those of $\hat{\Lambda}^0$. We can then interpret matrix \hat{A}^{-1} from WF, equation (33), as the initial (unperturbed) Green matrix, $\hat{G}^0 = \hat{A}^{-1}$, so that the rhs of the WF provides the *exact* expression for the resulting perturbed Green function (resolvent):

$$\hat{G} = (\lambda\hat{I} - \hat{\Lambda}^0 - \hat{U}\hat{V})^{-1} = \hat{G}^0 + \hat{G}^0\hat{U}\hat{C}^{-1}\hat{V}\hat{G}^0. \quad (34)$$

As the elements of \hat{C}^{-1} are inversely proportional to the determinant of the capacitance matrix,

$$C(\lambda) = \text{Det}\hat{C}(\lambda), \quad (35)$$

the new poles of the Green matrix, i.e. the new spectrum values, must be zeros of $C(\lambda)$.

It is pertinent to note here that of course the perturbative analysis above is just one of the possible variants of a general matrix perturbation theory (aside from applications to the crystal lattice theory [21]). Various perturbation techniques for generic tridiagonal Toeplitz matrices are addressed e.g. in [25–28].

4.2. A single inhomogeneity ('zero' bit) in a stable pattern

Now we can take the initial matrix $\hat{\Lambda}^0$ corresponding to the homogeneous cases from subsection 3.2 and consider local deviations from the uniform bit pattern. To employ WF (33), one needs to express the perturbation of the initial Green matrix $\hat{G}^0(\lambda)$, equation (28), in terms of the $\hat{U}\hat{V}$ -decomposition. Then by looking into the ensuing capacitance matrix, $\hat{C}(\lambda)$, we can obtain the localized eignemodes lying outside the unperturbed spectral band.

To consider the effect of rare 'zeros' in the pattern of 'unities', let us first address the case where there is a single 'zero' bit embedded into a uniform stable $\{1\}_N$ pattern: we denote such a pattern as

$$\{1 \dots \underbrace{0}_{s+1} \dots 1\}_N.$$

This means that the phase difference between the $(s + 1)$ th and s th solitons, $\Delta_1\delta_s$, is zero, while for all remaining sites these differences are equal to π . For simplicity, we assume that neither s nor $s + 1$ are the boundary sites of the train. As the deviation is local, the dynamical equations remain the same, see equations (24) and (25), except for those for the sites with numbers s and $s + 1$, for which our equations become

$$\begin{aligned} \frac{d^2w_s}{dz^2} &= w_{s-1} - w_{s+1} - 2 = \Delta_2w_s + 2w_s - 2w_{s+1} + f_s, \\ \frac{d^2w_{s+1}}{dz^2} &= w_{s+2} - w_s + 2 = \Delta_2w_{s+1} - 2w_s + 2w_{s+1} + f_{s+1}. \end{aligned} \quad (36)$$

The new nonzero components of the inhomogeneity vector are $f_s = -2$, $f_{s+1} = 2$. Mathematically, the system is very similar to that of the crystal lattice with a single defect bond. The perturbed Green matrix, $G_{mm'}(\lambda)$, can now be found by the use of perturbation analysis from subsection 4.1, the number of perturbed rows being two.

The $\hat{U}\hat{V}$ -decomposition of the perturbation emerging from equations (36) can be realized by the following two rectangular matrices:

$$\mathcal{U}_{kl} = (-1)^{l-1} [2\delta_{ks} - 2\delta_{ks+1}], \quad \mathcal{V}_{lk} = \delta_{ks}\delta_{l1} + \delta_{ks+1}\delta_{l2}, \quad (37)$$

where $l = 1, 2$; $k = 1 \dots N + 1$. The matrix of our perturbed linear system, equation (36), expressed through the unperturbed matrix $\hat{\Lambda}^0$ has the form $\hat{\Lambda} = \hat{\Lambda}^0 + \hat{U}\hat{V}$. The corresponding capacitance matrix reads

$$C_{lj} = \delta_{lj} + (-1)^j [2\delta_{l1}(G_{ss}^0 - G_{ss+1}^0) + 2\delta_{l2}(G_{ss+1}^0 - G_{s+1s+1}^0)], \quad k, j = 1, 2. \quad (38)$$

For the determinant of this capacitance matrix, we find the following expression:

$$C_s(\lambda) = 4G_{ss+1}^0(\lambda) - 2G_{ss}^0(\lambda) - 2G_{s+1s+1}^0(\lambda) + 1. \quad (39)$$

The equation $C_s(\lambda) = 0$ then implicitly defines the dependence of the eigenvalue for the unstable mode on the position s of the ‘defect’ bit: $\lambda = \lambda^*(s)$. The method above is ideologically similar to the Lifshitz criterion for finding localized impurity modes in the otherwise perfect 1D crystal [21]. The important difference of our case from that considered in [21] is that we deal with the ‘inelastic’ bond defect involving two sites rather than an isotopic defect considered by Lifshitz, which resulted in the rank 1 perturbation.

Now assuming $N \gg 1$, we can substitute in equation (39) the approximate expressions (29) for the elements of the unperturbed Green matrix, G_{ss}^0 etc. It means that the system becomes effectively semi-infinite and the index s numerates the distance of the defect site from the boundary. The magnitude of the new eigenvalue corresponding to the localized mode is exponentially close to $\lambda^* = 4/3$:

$$\lambda^*(s) = \frac{4}{3} \left(1 + \frac{32s}{27} 3^{-2s} \right) + o(3^{-2s}). \quad (40)$$

Already if one takes $s = 2$ (third bit from the boundary) the difference between the value $4/3$ and $\lambda^*(s)$ is of the order of 10^{-2} , so that the estimate $\lambda^* = 4/3$ is precise enough for our purposes. This means that for a low concentration of inhomogeneous bits, the instability rate can be evaluated as $\gamma^* \approx 2/\sqrt{3} \approx 1.15$. The numerical example of the 32 bit spectrum with a single ‘zero’ placed in the centre of the pattern is given in figure 2(a): one observes that the value of the unstable eigenvalue is indeed very close to $4/3$.

As the resulting driving vector $\mathbf{f}^* = 2(\delta_{s+1n} - \delta_{sn})$ now has two extra nonzero components, f_s and f_{s+1} , in addition to the boundary sites, it no longer possesses any particular symmetry and excites all the modes of the system including the unstable one. In the initial stage where $\gamma_k z \ll 1$, we can expand the functions $U_k^f(z)$ (17) up to the terms $\sim z^2$: $U_k^f(z) \sim z^2/2$. So the activation due to \mathbf{f}^* is

$$\mathbf{w} = z^2 \sum_k (v_k^{s+1} - v_k^s) \mathbf{v}_k, \quad (41)$$

and because of the orthogonality the only nonzero components are (up to z^2 , cf equation (31))

$$w_{s+1} = -w_s = z^2. \quad (42)$$

4.3. The width of the impurity mode: the case of small concentration of impurities

Because the perturbation in equations (36) affects only two sites, the corresponding unstable ‘impurity’ mode is localized on this perturbed bond as well, see figure 2(b). This effect is similar to the localization of phonon modes in a crystal lattice with an isotopic defect [21].

For the localized eigenvector \mathbf{v}_* corresponding to the eigenvalue $\lambda^*(s)$, we have

$$[\lambda^* \hat{I} - \hat{\Lambda}^0] \mathbf{v}_* = \hat{U} \hat{V} \mathbf{v}_*,$$

so we can write

$$v_*^n = G_{nk}^0(\lambda^*) [\hat{U} \hat{V}]_{km} v_*^m \quad (43)$$

(the summation over the repeated indices is assumed). Due to the structure of the perturbation $\hat{U} \hat{V}$, the expression on the rhs involves only v_*^s and v_*^{s+1} , which are to be treated as two linearly dependent constants. Indeed, from equation (43), one can write down the explicit expressions for v_*^s and v_*^{s+1} :

$$\begin{aligned} v_*^s &= 2G_{ss}^0 v_*^s - 2G_{ss+1}^0 v_*^{s+1}, \\ v_*^{s+1} &= -2G_{ss+1}^0 v_*^s + 2G_{s+1s+1}^0 v_*^{s+1}. \end{aligned} \quad (44)$$

The determinant of this system of linear algebraic equations coincides exactly with that for the capacitance matrix $C_s(\lambda^*)$ (35). Recall that $C_s(\lambda^*)$ is equal to zero (as it is the very definition of the localized eigenvalue) and hence equations (44) are linearly dependent. Then the spatial properties of v_*^n are determined by the behaviour of $G_{ns}^0(\lambda^*)$ (or $G_{ns+1}^0(\lambda^*)$, which is virtually the same for sites n distant from the defect, $|n - s| \gg 1$). One can pick the first equation from (44) and retaining e.g. v_*^s as an arbitrary (normalization) constant, $v_*^s = A = \text{const}$, we have $v_*^{s+1} = \beta_s A$, where we have introduced the notation

$$\beta_s = \frac{2G_{ss+1}^0(\lambda^*)}{2G_{ss}^0(\lambda^*) - 1},$$

which is also a constant for a given s . From equation (43) one then obtains

$$v_*^n = A \epsilon (1 - \beta_s) [G_{ns}^0(\lambda^*) - G_{ns+1}^0(\lambda^*)]. \quad (45)$$

We assume that the decay of the localized eigenvector has the form of the superposition of two exponents localized at s th and $(s + 1)$ th sites, but with the same decay rate R_s . The explicit ansatz for the v_*^n is as follows:

$$|v_*^n| = 2|A(1 - \beta_s)| \left[\exp\left(-\frac{|n - s|}{R_s}\right) - \exp\left(-\frac{|n - s - 1|}{R_s}\right) \right]. \quad (46)$$

Now comparing this expression with equation (45), we see that due to the form of v_*^n (46), the localization is attributed to the localization properties of the corresponding Green matrix elements. To get some explicit analytical results let us assume that $N \gg 1$, and therefore we can use the simplified integral expression for the Green matrix of the self-infinite system, equation (29). Next we suppose that $|n + s| \gg 1$ and $|n - s| \ll |n + s|$. Then inasmuch as $|F(\lambda^*)| < 1$, $F(\lambda)$ being defined by equation (30), one can drop the second summand $\sim F(\lambda^*)^{n+s+1}$ in equation (29). After that one arrives at the approximate expression for the localization length R^* (for s being far from the system edge) in the form

$$R^* \approx -\frac{1}{\ln |F(\lambda^*)|} = 0.91, \quad (47)$$

i.e. the ‘defect’ modes are rather well localized. The estimate above helps one to extend the results for a single ‘defect’ bit to the case of sparse ‘zeros’ in the pattern of ‘unities’: if we introduce a small number of such ‘defects’ that are distant from each other, one still expects the results of subsection 4.2 to hold. For the correctness of this, we must ensure that the concentration of the ‘defect bits’, c , satisfies the inequality: $c \ll c^* = (2R^*)^{-1}$.

One such pattern with the concentration of regularly placed defect bits $c = 1/5$ is given in figure 2(c): one can observe a pronounced narrow band of unstable modes with $\lambda \approx \lambda^* = 4/3$.

4.4. Some remarks on general bit patterns

In the general case, we have an equal probability to meet either ‘zero’ or ‘unity’ (unless some specific source encoding format is used). If ‘zeros’ are sparse, than each ‘zero’ bit corresponds to an unstable mode growing with the increment close to $\sqrt{\lambda^*} = 2/\sqrt{3}$, see figure 2(c), and this eigenmode has an asymmetric peak localized at a defect. As the concentration of ‘zeros’ increases, the analysis above does not apply. Figure 2(d) shows a particular randomly generated pattern with the average concentration of zeros $c = 1/2$, which displays a mixture of stable and unstable modes without any specific ordering. The characteristic disintegration time of the pulse train is given by the highest positive eigenvalue λ_{\max} ; it corresponds to the eigenmode with the largest growth increment $\gamma_{\max} = \lambda_{\max}^{1/2}$.

The domain of location of the eigenvalues in the arbitrary case can be estimated via the Gershgorin theorem [29], which states that for an arbitrary $N \times N$ symmetric matrix (say $\hat{\Lambda}$) the real eigenvalues occupy the union of N intervals, each defined by the inequalities:

$$|\lambda - \Lambda_{ii}| \leq \sum_{j \neq i}^N |\Lambda_{ij}|, \quad i = 1, \dots, N. \quad (48)$$

Substituting the explicit values of the elements for our $\hat{\Lambda}$, equation (9), we observe that for any given pattern the eigenvalues belong to the band $[-4, 4]$: the region between the minimal value of λ for pure ‘unities’, -4 , and maximal for uniform ‘zeros’, 4 .

Further properties of the spectra of arbitrary bit patterns follow from the general theory of tridiagonal matrices [29]: since all sub-diagonal elements are always non-zero, the spectrum is non-degenerate. Also, by inverting the bit pattern, $\{b\}_N \rightarrow \{1 - b\}_N$, the eigenvalues change sign, so it is sufficient to study half of the patterns, where the number of ‘zeros’ is less than or equal to the number of ‘unities’.

Finally, not all the unstable eigenmodes of matrix Λ are excited but only those which are not orthogonal to the driving vector \mathbf{f} , equation (11). Therefore, the problem of finding the optimal encoding for error-free transmission can be reformulated in terms of finding such patterns (i.e. encoding formats) which minimize the projections f_k of the unstable eigenmodes onto the driving term \mathbf{f} .

5. Nonlinear regime

In the previous section, we considered the linearized dynamics of the CTC, which is valid at the initial stage of the evolution. However, as the CTC is integrable by the inverse scattering transform we can also establish its behaviour at longer distances compared to those where the linearization approach of section 3 is valid [10, 13], and how it depends on the input bit pattern. It can be done by exploiting the fact that the eigenvalues of the so-called Lax scattering matrix are the integrals of motion due to the CTC integrability. Then if one determines these Lax matrix eigenvalues from the initial conditions, the long-distance properties are determined by the distribution of these eigenvalues. This auxiliary eigenproblem for the CTC is generally non-Hermitian, and thus differs from the eigenproblem for the linearized dynamical equations considered previously. We would like to stress again here that the CTC itself describes well the true NLSE dynamics only for a sufficient interpulse separation. Because of this the long-time behaviour of the train cannot be correctly described by the CTC for a general initial distribution, see [12, 16]. However, the results of this section are exact for the CTC itself and can be applied to the NLSE when the correspondence between the dynamics of two models is good enough [16].

5.1. Lax representation of CTC

Since equation (6) is integrable by the inverse scattering transform, it allows representation in terms of the Lax pair [10, 13]:

$$\frac{d\hat{L}}{dz} = [\hat{\Theta} \hat{L}]. \quad (49)$$

The explicit form of the matrix $\hat{\Theta}$ is insignificant for our considerations, but the (generally complex) Lax matrix \hat{L} has a tridiagonal symmetric structure defined by the expression:

$$L_{ij} = \sum_{k=1}^N [B_k \{E_{ij}\}_{kk} + A_k (\{E_{ij}\}_{k,k+1} + \{E_{ij}\}_{k+1,k})]. \quad (50)$$

Matrix \hat{E} is a matrix of matrices with elements expressed via the Kronecker symbols, $\{E_{ij}\}_{km} = \delta_{ik}\delta_{jm}$ (and additionally $\{E_{ij}\}_{km} \equiv 0$ if either of indexes exceeds the range of the chain), and for A_k and B_k , we have

$$A_k = \frac{1}{2} e^{(q_{k+1}-q_k)/2}, \tag{51}$$

$$B_k = \frac{1}{2}(\mu_k + i\nu_k). \tag{52}$$

Again we assume that the amplitudes of the solitons are the same, $\nu_k = \nu$, and the velocities are zero, $\mu_k = 0$. Then all B_k are constants, $B_k = B = i\nu/2$, and all diagonal elements of \hat{L} , equation (50), are the same and equal to B . Subtracting these diagonal B , we will deal only with the reduced matrix (we also denote it by \hat{L}):

$$L_{ij} = \sum_{k=1}^N A_k [\{E_{ij}\}_{k,k+1} + \{E_{ij}\}_{k+1,k}]. \tag{53}$$

The details of the CTC dynamical regimes classified through the eigenvalues $l_k = \kappa_k + i\zeta_k$ of the Lax matrix \hat{L} , are given in [10–13], and we will not reproduce these results here.

5.2. The structure of \hat{L} matrix for an arbitrary DPSK bit pattern and homogeneous cases

Let us again assume that there are $N + 1$ solitons employed to transmit a $\{b_1, \dots, b_N\}_N$ bit pattern, the solitons being initially equispaced with the spacing r . Then the coefficients A_k from equation (51) have the form

$$A_k = (a/2) \sqrt{\sigma_{k+1}}, \quad k = 0, 1, \dots, N - 1, \quad A_N = 0, \tag{54}$$

where we have used the notations a and σ_k from subsection 3.1. The matrix \hat{L} (53) has the following structure (we use the reduced matrix with the subtracted constant diagonal elements [13]):

$$\hat{L} = \frac{a}{2} \begin{pmatrix} 0 & \sqrt{\sigma_1} & 0 & 0 & \dots & 0 & 0 & 0 \\ \sqrt{\sigma_1} & 0 & \sqrt{\sigma_2} & 0 & \dots & 0 & 0 & 0 \\ 0 & \sqrt{\sigma_2} & 0 & \sqrt{\sigma_3} & \dots & 0 & 0 & 0 \\ \dots & \dots \\ \dots & \dots \\ \dots & \dots \\ 0 & 0 & 0 & 0 & \dots & \sqrt{\sigma_{N-1}} & 0 & \sqrt{\sigma_N} \\ 0 & 0 & 0 & 0 & \dots & 0 & \sqrt{\sigma_N} & 0 \end{pmatrix}. \tag{55}$$

We will omit the factor $a/2$ in the definition of the Lax matrix since it can be absorbed by rescaling the distance: $az/2 \rightarrow z$. We can now study the dynamical regimes for the same patterns as were considered in section 3. The spectral dependences and corresponding eigenvectors of these marginal input patterns are a particular realization of the general homogeneous case considered in [10].

For pure ‘zeros’, we have $\sigma_n = -1$, and \hat{L} is skew-Hermitian. We shall label the corresponding matrix (55) with the superscript ‘0’: \hat{L}^0 . The eigenspectrum is purely imaginary and given by

$$l_k = 2i \cos \tilde{\rho}_k, \quad \tilde{\rho}_k = \frac{\pi k}{N + 2}, \quad k = 1, \dots, N + 1. \tag{56}$$

For pure ‘unities’, all $\sigma_n = 1$, and the matrix \hat{L} is Hermitian. The spectrum is real and given by

$$l_k = 2 \cos \tilde{\rho}_k, \quad k = 1, \dots, N + 1. \tag{57}$$

The normalized eigenvectors for both patterns are

$$v_k^n = \sqrt{\frac{2}{n+2}} \sin[\tilde{\rho}_k(n+1)], \quad k = 1, \dots, N+1, \quad n = 0, \dots, N, \quad (58)$$

and the Green matrix is (we mark it with a calligraphical letter for distinguishing from the expressions referring to the linear regime)

$$\hat{\mathcal{G}}_{mm'}^0 = (l - \hat{L}^0)^{-1}_{mm'} = \frac{2}{N+1} \sum_{k=1}^{N+1} \frac{\sin[\tilde{\rho}_k(n+1)] \sin[\tilde{\rho}_k(n'+1)]}{l - l_k}. \quad (59)$$

In the limit of large N (semiinfinite system), we can again use the continuum approximation instead of the sum. Then for the $\{0\}_N$ pattern with the dispersion relation (56), we have

$$\begin{aligned} \hat{\mathcal{G}}_{mm'}^0 &\approx \frac{2}{\pi} \int_0^\pi \frac{\sin[\rho(n+1)] \sin[\rho(n'+1)]}{l - 2i \cos \rho} d\rho \\ &= -\text{Sign}(\text{Re}[l]) \frac{i}{\sqrt{l^2 + 4}} (Z(l)^{|n-n'|} - Z(l)^{n+n'+2}), \end{aligned} \quad (60)$$

where $\text{Sign}[\dots]$ means the signum function and

$$Z(l) = \begin{cases} -\frac{i}{2}(l + \sqrt{l^2 + 4}) & \text{for } \text{Re}[l] < 0, \\ -\frac{i}{2}(l - \sqrt{l^2 + 4}) & \text{for } \text{Re}[l] > 0. \end{cases}$$

5.3. A single ‘unity’ in the pattern of ‘zeros’

One can employ the matrix perturbation analysis from section 4.1 and start with the pattern $\{0\}_N$, for example, studying the appearance of states with non-zero real parts of the eigenvalues. In this section, we assume that the bit number $s+1$ is flipped from ‘zero’ to ‘unity’, so that $\sigma_s = 1$, while the rest of bit indicators are equal to -1 .

We begin with the $\hat{U}\hat{V}$ -factorization of the perturbation to the \hat{L}^0 matrix. For our perturbed matrix we have $L_{s+1s} = L_{ss+1} = 1$, and matrices \hat{U} and \hat{V} can be introduced as follows:

$$U_{kj} = \gamma[\delta_{j1}\delta_{ks+1} + \delta_{j2}\delta_{ks}], \quad V_{jk} = \delta_{ks}\delta_{j1} + \delta_{ks+1}\delta_{j2}, \quad (61)$$

where $\gamma = 1 - i$; indexes $j = 1, 2$, and $k = 1 \dots N+1$. The resulting $(N+1) \times (N+1)$ perturbation matrix $\hat{U}\hat{V}$ is zero except for the elements with indices $(s, s+1)$ and $(s+1, s)$, which are equal to γ . The capacitance matrix (32) based on the Green matrix for \hat{L}^0 , equation (59), can be readily calculated as

$$C_{jl} = \delta_{jl}(1 - \gamma\hat{\mathcal{G}}_{ss+1}^0) - \gamma(\hat{\mathcal{G}}_{ss}^0\delta_{j1}\delta_{l2} + \hat{\mathcal{G}}_{s+1s+1}^0\delta_{j2}\delta_{l1}), \quad (62)$$

where $j, l = 1, 2$, and we have accounted for the symmetry of the Green function (59): $\hat{\mathcal{G}}_{ss+1}^0 = \hat{\mathcal{G}}_{s+1s}^0$. The corresponding determinant $C_s(l)$ is

$$C_s(l) = (1 - \gamma\hat{\mathcal{G}}_{ss+1}^0)^2 - \gamma^2\hat{\mathcal{G}}_{ss}^0\hat{\mathcal{G}}_{s+1s+1}^0, \quad (63)$$

and by using the approximation of the semi-infinite system for the explicit calculation of sums, equation (60), one can find out the new spectral values, which have arisen due to the presence of a single ‘unity’. Note that since \hat{L} is a non-Hermitian matrix, there exist several new complex roots of the equation $C_s(l) = 0$. The number of new roots is determined by the value of s . In figures 3(a) and (b), we depict the contour plots for $\text{Re}[C_s(l)] = 0$ (solid lines) and $\text{Im}[C_s(l)] = 0$ (dashed lines) for the particular cases $s = 5$ and $s = 10$. The points where these curves cross each other correspond to the new spectrum points, i.e. to the roots of $C_s(l) = 0$. One observes that the spectrum now is highly sensitive to the value of s . In the same plots, we show the numerical results for the 512 bit pattern with the same location of the

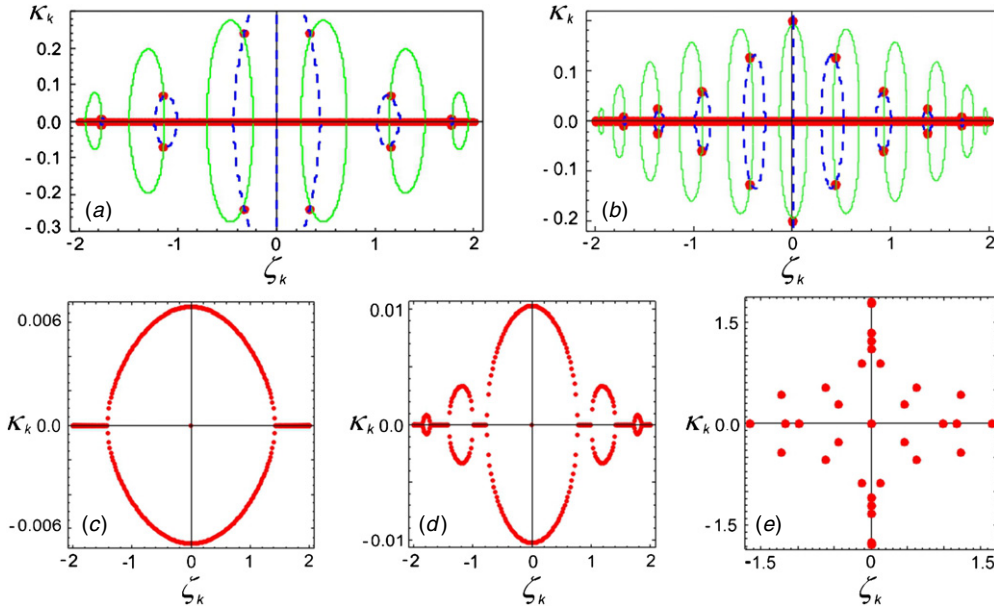


Figure 3. Some typical spectra of complex eigenvalues, $l_k = \kappa_k + i\zeta_k$, for the Lax matrix \hat{L} (the plots are rotated 90°). The upper row corresponds to a single ‘unity’ placed near the edge of the 512 bit pattern of ‘zeros’: for (a) the position of the ‘unity’ is $s + 1 = 6$, and for (b) $s + 1 = 11$. The solid and dashed lines are the level curves for the determinant of the capacitance matrix for the semi-infinite system with the same defect placement, (63): the solid line is the contour plot for $\text{Re}[C_s(l)] = 0$, the dashed—for $\text{Im}[C_s(l)] = 0$; the intersections of these curves give the locations of the new eigenvalues, defined by $C_s(l) = 0$. Panels (c) and (d) illustrate the sensitivity of the Lax spectra to the position of the defect: for the panel (c) the defect is placed at $s + 1 = N/2 + 2 = 258$, for the panel (d)—at $s + 1 = N/2 + 4 = 260$. The last panel (e) displays the distribution corresponding to the same realization of a random 32 bit sequence as shown for the linear case, see figure 2(d): it demonstrates all the typical symmetries leading to the complex regimes described in section 5.4.

‘defect bit’ (large dots): the results are in a good agreement with the theory. In general, the spectrum of \hat{L} is very sensitive to the location of the ‘defect bit’ in the train, and it is impossible to derive a simple general formula encompassing all possible cases. Figures 3(c) and (d) also demonstrate this sensitivity when the defect is located near the centre of the pattern.

5.4. General inhomogeneous patterns in the nonlinear regime

Let us outline the symmetry properties of the eigenspectrum for the matrix \hat{L} , equation (55), regarding an arbitrary input bit pattern. Let us denote by $P_{N+1}(l)$ the characteristic polynomial of matrix (55). Then we have the following recurrence relation:

$$P_{N+1}(l) = -lP_N(l) - \sigma_N P_{N-1}(l), \quad P_0 = 1, \quad P_1 = -l.$$

The coefficients of $P_{N+1}(l)$ are always real, so if l_k is an eigenvalue, its complex conjugate, \bar{l}_k , is also an eigenvalue. Additionally, $P_{N+1}(l)$ contains only either even or odd powers of l , corresponding to the parity of $N + 1$, respectively (the patterns with the even bit number always have a zero eigenvalue). This means that it is enough to plot the complex spectra only in the first quadrant of the complex plane l : the rest follows by a combination of mirror reflections with respect to both axes. The Gershgorin theorem [29] is applicable to the complex matrix \hat{L} as well, but instead of Gershgorin intervals one needs to consider the union of Gershgorin discs

formally defined in the same fashion as in equation (48). This gives the domain of localization of the eigenvalues: $|l| \leq 2$. The spectrum for a random 32 bit pattern is shown in figure 3(e). It displays all the characteristic symmetries of an arbitrary eigenvalue distribution.

Let us mention some spectral properties ensuing from the aforementioned symmetries. Firstly, let us formulate a *duality principle* for the phase-coded CTC input. Suppose that we have an arbitrary sequence in the form of the DPSK phase-coded input, which yields a corresponding eigenvalue portrait of the reduced scattering matrix \hat{L} , equation (55). Then, if one flips ‘zeros’ and ‘unities’, the Lax matrix is transformed as $\hat{L} \rightarrow i\hat{L}^\dagger$, and the eigenvalues distribution of the new pattern is obtained by flipping the original distribution with respect to the bisector $\kappa = \zeta$. The corresponding asymptotic regime is then ‘flipped’ accordingly.

Secondly, based on the classification from [12], we can establish the regimes occurring for a generic CTC DPSK-coded pattern. Generally, each asymptotic regime of the CTC lattice has a direct counterpart in the dynamics of NLSE soliton train (valid of course when the CTC is applicable, i.e solitons are well separated). One can discern the following three types of solution complexes.

- A *quadruplet* corresponding to the set of four complex eigenvalues, $\pm l_k$ and $\pm \bar{l}_k$. Each quadruplet corresponds to the two bound pairs of solitons moving with the same velocity in the opposite directions.
- A *breather* corresponding to the pair of purely imaginary eigenvalues $\pm i\zeta_k$. The breathers make up the nondispersive part of the solution.
- *Asymptotically free pairs* of solitons moving with equal velocities in the opposite directions.

Note that under some special conditions like e.g. a 3-pulse breather [12], the solutions of the CTC can become singular. When such solutions approach singularity, the CTC model of course ceases to apply to the NLSE pulse trains and one has to resort to direct numerical simulations. The reader is referred to references [12, 13] for the general discussion of these solutions. A generic pattern like the one corresponding to figure 3(e) will have all three constituents: its asymptotic behaviour corresponds to a complicated mixture of the regimes above which represents a refined classification from [13], now taking into account the specific symmetries introduced by the binary DPSK encoding of the phase.

6. Some remarks on the practical applications of the method

6.1. Evaluation of scales

The method considered here can be used e.g. for the direct evaluation of various dynamical scales related to the evolution of the soliton train.

In particular, one often wants to estimate the characteristic error-free propagation distance, z_{err} , in the *linear regime*. For illustrative reasons, let us consider a generic bit pattern of 33 solitons where we randomly encoded 32 bits: we use the same realization of a random bit pattern as in figure 2(d) (and figure 3(e) as well). For this pattern, one finds the largest positive eigenvalue for the spectrum of the linearized model: $\lambda_{\text{max}} \approx 3.57$. Fixing the parameters of the transmission, say $2\nu = 1$, $r = 5$, we scale the distances back into the soliton units and obtain the growth rate: $\gamma_{\text{max}} = 8\nu^2 e^{-r\nu} \sqrt{\lambda_{\text{max}}} \approx 0.31$. So, the value $z_{\text{err}} = \gamma_{\text{max}}^{-1} \approx 3.23$ defines the scale beyond which the immediate values of soliton positions for given transmission parameters become significantly different from the initial distribution. Simultaneously, z_{err} sets the limit for the applicability of the linear analysis. Note that the (scaled back) forcing amplitudes in equation (8), which govern the development of instabilities, are small: $|f_n| \sim (4\nu a)^{-2}$, so that

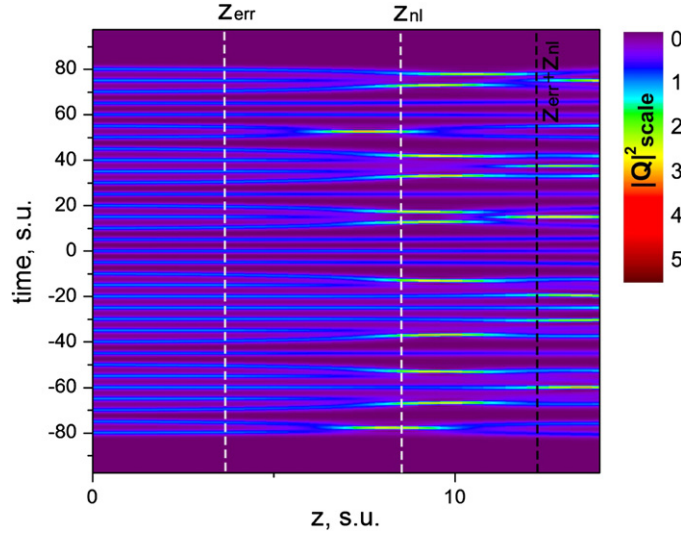


Figure 4. The density plot of $|Q(z, t)|^2$ obtained by the numerical integration of NLSE (1), which corresponds to the propagation of the randomly DPSK-encoded 32 bit soliton train. The initial phase distribution is the same as was used in figures 2(d) and 3(e). The explanation for the corresponding z -scales z_{err} and z_{nl} is given in the text. Both time and propagation distance are measured in soliton units (s.u.).

the unstable exponentials are multiplied by small factors and the aforementioned limits are offset somewhat. In figure 4, we show the dynamics of the chosen 32 bit pattern (obtained by the direct numerical simulation of NLSE), and the estimate for the z_{err} for the linear regime and error-free distance obtained above is visually in a good agreement with the real physical situation. Let us provide some real world units estimate of the error scale, for which we should multiply z_{err} by the dispersion length z_0 , which is in turn defined as [3]

$$z_0[\text{m}] = 6.07 \times 10^2 \frac{\tau^2[\text{ps}]}{\lambda_w^2[\mu\text{m}]D[\text{ps}/(\text{nm} \cdot \text{km})]},$$

where λ_w is the carrier wavelength, τ is the pulse width and D is a group velocity dispersion. For the typical values used in the transmission: $\tau = 15$ ps, $\lambda_w = 1.55$ μm and $D = 0.5$ ps(nm km)⁻¹, we have $z_0 \approx 115$ km, and z_{err} in real units amounts to 371.5 km. Now we can define the same scale, z_{err}^* but for the ‘rare bit’ format, when the concentration of ‘zeros’ satisfies $c \ll c^* \approx 0.55$. The typical spectrum now has a narrow instability band concentrated around $\lambda^* = 4/3$, see figure 2(c). When we perform the reverse scaling back to the soliton units, we obtain a universal estimate:

$$z_{\text{err}}^* = \frac{\sqrt{3} e^{r\nu}}{16 \nu^2}. \tag{64}$$

Setting the same values for $\nu = 0.5$ and $r = 5$ as in the previous paragraph, one arrives at the larger value of z_{err} than that for a pattern above: $\gamma_{\text{max}}^* \approx 0.19$, $z_{\text{err}}^* \approx 5.28$ or 607.2 km in the real world units. The overall idea underlying the improvement of the quality of information transmission consists in suppressing the excitation of instable eigenmodes and reducing their projections onto the driving vector \mathbf{f} , equation (8), by means of a more sophisticated encoding scheme. For the distances more than z_{err} , the nonlinear effects come into play and we can define the measure of information distortion during the intermittent evolution only by considering the exact CTC solutions (or, when the CTC is inapplicable, one must consider the NLSE (1)

itself). For these evolution distances, the CTC solution evolves into a mixture of nonlinear regimes (see [13] and the previous chapter). For the illustrative reasons we can again use the eigenvalues portrait corresponding to the random bit-pattern from figure 3(e), which contains all peculiarities pertinent to a general case. Now one can pose the question: when will at least one of the pulses walk off from the prescribed slot and an error will definitely occur? At this point we note that within the simplified CTC model, there are two possible sources of error. First of all, we have solitons (or soliton clusters) which behave as ‘free Toda particles’ moving out from their slots—an effect which is within the range of applicability of CTC as long as the pulses are well separated. But there also exists another type of distortion of the train when one or more solitons collide and coalesce. The latter can occur for both oscillating modes corresponding to breather states and for singular solutions of CTC [12]. Such collision effects represent another possible source of error which is however beyond the scope of the CTC model and is not discussed here. What we will be concerned with is the scale, z_{nl} , which represents an *upper bound on error-free transmission* due to ‘free Toda particle’ instability only. Because it takes into account only one type of error source, it cannot simultaneously serve as the lower bound for such a distance (because errors of other type might most probably have occurred earlier) but nevertheless our numerical results show that the bound is remarkably tight (see below).

To get an estimate of this distance, we resort to considering the complex eigenvalues l_k of the matrix \hat{L} . We assume that the escape rate corresponds to individual solitons (or soliton complexes) moving away from the slot centre, i.e. having nonzero κ_k . In order to obtain z_{nl} , one finds the value of the largest real part among all eigenvalues, $\kappa_{\text{max}} = \max \text{Re}[l_k]$. For our example pattern, figure 3(e), we obtain $\kappa_{\text{max}} = 1.78$. The quantity $4\nu e^{-r\nu} \kappa_{\text{max}}$ gives the asymptotic ‘velocity’, $V = d\xi/dz$, of the fastest moving soliton (soliton complex). Then we estimate the ‘time’ for the soliton to cover half of the distance separating it from the adjacent slot, i.e. $r/2$: $z_{\text{nl}} = r/(2V)$. For the previously used values, $\nu = 1$, $r = 5$, this gives the estimate: $z_{\text{nl}} = (r e^{r\nu}/8\nu\kappa_{\text{max}}) \approx 8.6$. Note that it is meaningless to apply the values of z_{nl} that are close to or less than z_{err} , as the nonlinear regime occurs only after the linear stage.

The considerations based on the lattice-type approach developed in the current work can be applied to a soliton pattern of an arbitrary length and bit composition. To get the characteristic boundaries of linear and nonlinear regimes corresponding to a given pattern, one only needs to analyse two linear, sparse eigenvalue problems, (9) and (55). The numerical procedure is computationally much less expensive than simulating the original NLSE, equation (1). Indeed, for the current approach one should assign a single (complex) degree of freedom to each bit, instead of resolving numerically each pulse on a mesh with a number of points for each soliton. The further improvement is that although the eigenvalue decomposition of a general matrix requires $O(N^3)$ operations, for the tridiagonal matrices the actual cost is only $O(N^2)$ operations. Finally, when general estimates are sufficient one can use the Gershgorin bounds: for an arbitrary pattern in the linearized case, the maximum positive eigenvalue $\lambda_{\text{max}} < 4$, which gives the minimum possible error-free propagation distance as $z_{\text{err}} \sim e^{r\nu}/16\nu^2$. As for the \hat{L} matrix, the maximum real part of an eigenvalue is $\kappa_{\text{max}} < 2$, so that the distance z_{nl} can be estimated as $Z_{\text{nl}} \sim r e^{r\nu}/16\nu$. Note that both distances scale exponentially with the parameter $r\nu$ (but the requirements $e^{-r\nu} \ll 1$ must be fulfilled in order for the CTC model to apply).

6.2. Simulation of the NLSE using the random and ‘rare-bits’ input phase encoding

In order to check further how the results of the linear analysis based on the CTC, equation (6), comply with the true dynamics of a given pattern we performed additional

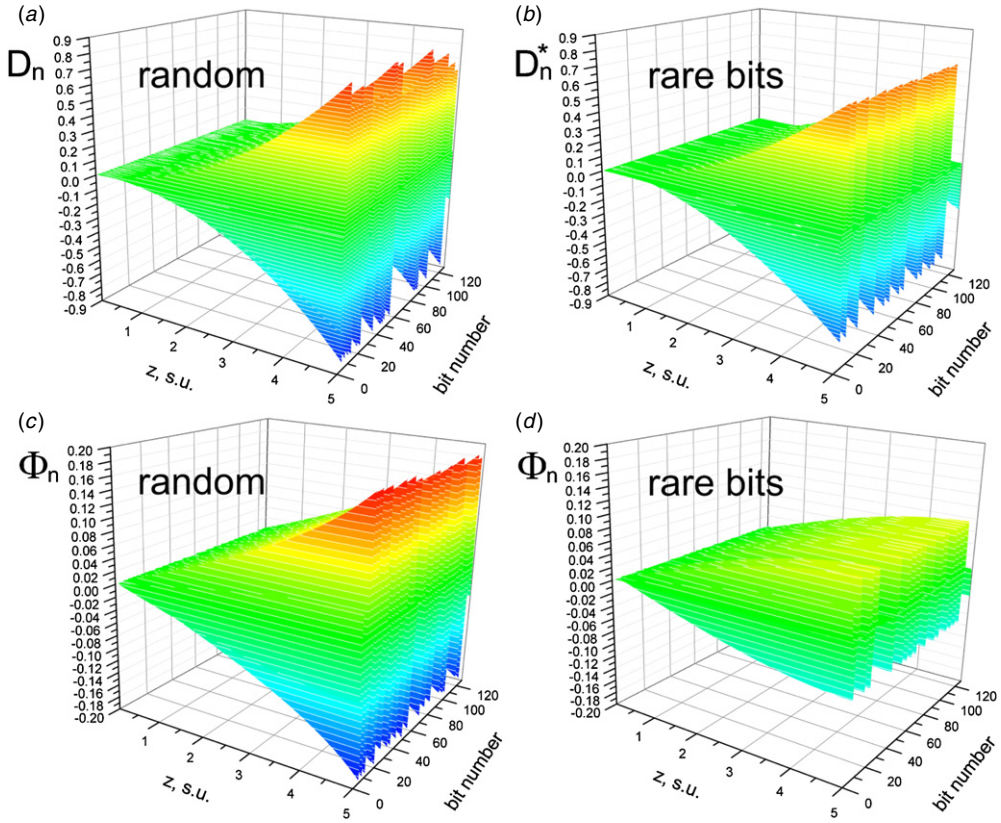


Figure 5. Dynamics of timing D_n and phase Φ_n jitters, defined by equations (67) (or D_n^* , equation (69), for the timing jitter of the ‘rare bits’ format), and (68) respectively, obtained by the direct integration of the initial NLSE (1). For the input in panels (a) and (c) we used a random 128-bit pattern with equal probability for each bit value to be either ‘0’ or ‘1’, for panels (b) and (d)—the 128-slots ‘rare bits’ encoding with each fifth bit encoded with equal probability to be either ‘0’ or ‘1’. The propagation distance z is measured in soliton units (s.u.).

numerical simulations of the original NLSE (1) with the input in the form of either a completely random DPSK-coded soliton train or DPSK-code based on the ‘rare-bits’ format. In every run, we used the initial pattern of well-separated solitons with equal amplitudes $2\nu = 1$ and initial intersoliton separation $r = 5$ (both quantities are in soliton units, see section 2).

A straightforward way of defining phases and positions of individual solitons could be to use the inverse scattering transform method utilizing the integrability of NLSE [1]. However for our situation that would overcomplicate the problem as the solitons remain well separated in the following simulation runs (figure 5). Therefore one can use simpler definitions for the positions and phases of individual solitons defined via the averaging over the individual slots [30]:

$$\bar{\xi}_n(z) = \frac{\int_{\tau_n} dt t |Q(z, t)|^2}{\int_{\tau_n} dt |Q(z, t)|^2} + r n, \tag{65}$$

$$\bar{\delta}_n(z) = \tan^{-1} \frac{\int_{\tau_n} dt \text{Im}[Q(z, t)] |Q(z, t)|^2}{\int_{\tau_n} dt \text{Re}[Q(z, t)] |Q(z, t)|^2} - \delta_n(0). \tag{66}$$

Here the designation $\int_{t_n} dt \dots$ means the integration of the corresponding quantity over the n th symmetric slot of width r centred at the initial position of the n th soliton, rn . While the slots are rigidly fixed, each of the solitons experiences a complicated motion within each slot or walks beyond it. In the latter case, of course, the definitions above lose their sense but insofar as the simulations are performed for the weak deviations of the initial positions, one does not need to deal with these more difficult cases.

In figure 5, we depict the evolution of the relative soliton position and phase deviations (i.e. timing and phase jitters, respectively), defined as

$$D_n(z) = \frac{\bar{\xi}_{n+1}(z) - \bar{\xi}_n(z)}{r}, \quad (67)$$

$$\Phi_n = \frac{\bar{\delta}_{n+1}(z) - \bar{\delta}_n}{\pi}. \quad (68)$$

These quantities correspond to the dynamics of real and imaginary parts of $\Delta_1 q_n$ from equation (6). We compare the dynamics of timing and phase jitters for an entirely random 128-bit pattern, panels (a) and (c), and for the ‘rare bits’ format with the same 128 slots, panels (c) and (d). The latter was discussed in sections 4.2 and 4.3, and predicted to be more robust compared to the completely random case. In this regime, the number of repelling solitons largely exceeds the number of attracting ones and we have a quadratic contribution $\sim \epsilon_{\text{sp}} z^2$ of the stable modes; see the end of section 3.2 and equation (42). We can then introduce an explicit correction in the jitter definition (67) with the ‘antidrift’ term making positive and negative jitters balanced:

$$D_n^*(z) = \frac{\bar{\xi}_{n+1}(z) - \bar{\xi}_n(z)}{r} - \epsilon_{\text{sp}} z^2, \quad (69)$$

where $\epsilon_{\text{sp}} \approx 2$ in the rescaled units of section 3.2 (≈ 0.03 in the soliton units). This new renormalized quantity now accounts only for the genuine instability occurring due to the appearance of the rare inhomogeneous bits.

Comparing figures 5(a) and (c), one can see that the utilization of the ‘rare bits’ encoding gives roughly 20% reduction in the timing jitters (deviation of the relative initial soliton positions). As to the phase jitters (relative deviations from the initial phase distribution), see figures 5(b) and (d), those are activated due to the nonlinearity of the initial CTC. Their values are smaller as compared to the timing jitters, and the advantage of using the ‘rare bits’ encoding already accounts for more than 60% reduction.

7. Conclusion

To sum up, we have studied the analogy between crystal lattice dynamics as occurring in condensed matter physics and the dynamic lattice of nonlinearly interacting solitons. The initial point was to utilize an established method that reduces the dynamics of the position and phase for each soliton to the integrable complex Toda chain. We have then studied how the particular symmetries imposed by the DPSK encoding used in optical telecommunications (where the phase difference between the adjacent solitons is either 0 or π) affect the dynamics of a pattern in the two propagation regimes: initial propagation described by the linearization of the CTC and the nonlinear behaviour at larger propagation distances. In the latter limit, the CTC generally ceases to apply to the NLSE pulse trains; however, we provide the approximate upper bound for the error-free transmission which is due to the escape of ‘free Toda particles’. This escape can still be estimated within the framework of the CTC. In both regimes, the study was reduced to classifying the eigenvalues of a certain tridiagonal matrix: the real symmetric

one for the case of linearized dynamics, and the complex symmetric Lax matrix for the long haul propagation. The DPSK encoding (binary phase encoding of the adjacent pulses) scheme imposes additional symmetries onto the eigenvalue distribution of these matrices. Firstly, we established the behaviour at the initial stage of evolution and quantified the inflation and deflation of intra-pulse distances. Consequently, we applied matrix perturbation theory (in the form of Woodbury formula) to obtain analytical results for some types of bit patterns using the analogy with the phonon lattices in the condensed matter physics. We demonstrated that in order to minimize the distortion of information and create an optimal bit encoding format, one needs to suppress the unstable modes by reducing their projection onto the driving forcing vector of the linearized dynamical system. It has to be noted that the proposed ‘rare bits’ encoding format (where only a small fraction of the pulses encodes information) is just the illustration of the idea that one can manipulate the properties of the train by imposing some specific constraints on phase modulation. The resulting properties referring to the format stability and characteristic scales can be analysed by means of the lattice-type approach. Then we studied the dynamical properties of a soliton train at larger propagation distances. We considered some characteristic bit patterns and identified the common mechanisms of information distortion. Additionally, we classified the emerging asymptotic dynamical regimes according to the symmetries of the bit patterns, and specified universal bonds on the soliton escape length.

Acknowledgments

The authors are grateful to Professor Sergey Gredeskul for valuable comments. This work was supported by the EPSRC.

References

- [1] Manakov S V, Novikov S P, Pitaevskii L P and Zakharov V E 1984 *Theory of Solitons* (New York: Consultants Bureau)
- [2] Zakharov V E and Shabat A B 1972 *Sov. Phys.—JETP* **34** 62–9
- [3] Hasegawa A and Kodama Y 1995 *Solitons in Optical Communications* (Oxford: Oxford University Press)
- [4] Gnauk A H and Winzer P J 2005 *J. Lightwave Technol.* **23** 115–30
- [5] Winzer P J and Essiambre R J 2006 *Proc. IEEE* **94** 952–85
- [6] Winzer P J and Essiambre R J 2006 *J. Lightwave Technol.* **24** 4711–28
- [7] Peleg A 2004 *Opt. Lett.* **29** 1980–2
- [8] Sanchez A and Bishop A R 1998 *SIAM Rev.* **40** 579–615
- [9] Karpman V I and Solovov V V 1981 *Physica D* **3** 487–502
- [10] Gerdjikov V S, Kaup D J, Uzunov I M and Evstatiev E G 1996 *Phys. Rev. Lett.* **77** 3943–6
- [11] Gerdjikov V S, Uzunov I M, Evstatiev E G and Diankov G L 1997 *Phys. Rev. E* **55** 6039–60
- [12] Gerdjikov V S, Evstatiev E G, Kaup D J, Diankov G L and Uzunov I M 1998 *Phys. Lett. A* **241** 323–8
- [13] Gerdjikov V S, Evstatiev E G and Ivanov R I 1998 *J. Phys. A: Math. Gen.* **31** 8221–32
- [14] Arnold J M 1998 *J. Opt. Soc. Am. A* **15** 1450–8
- [15] Arnold J M 1999 *Phys. Rev. E* **60** 979–86
- [16] Gerdjikov V S, Doktorov E V and Yang J 2001 *Phys. Rev. E* **64** 056617
- [17] Doktorov E V, Matsuka N P and Rothos V M 2004 *Phys. Rev. E* **69** 056607
- [18] Gerdjikov V S, Baizakov B B, Salerno M and Kostov N A 2006 *Phys. Rev. E* **73** 046606
- [19] Shchesnovich V S 2002 *Phys. Rev. E* **65** 046614
- [20] Gerdjikov V S, Kostov N A, Doktorov E V and Matsuka N P 2009 *Math. Comput. Simul.* **80** 112–9
- [21] Kosevich A M 1999 *The Crystal Lattice: Phonons, Solitons, Dislocations* (Berlin: Wiley-VCH)
- [22] Hager W W 1989 *SIAM Rev.* **31** 221–39
- [23] Woodbury M 1950 Inverting modified matrices *Memorandum Report 42* (Princeton, NJ: Statistical Research Group, Princeton University)

- [24] Prylepskiy Y E, Derevyanko S A and Turitsyn S K 2010 *MMET: Int. Conf. Mathematical Methods in Electromagnetic Theory (Kyiv)* (IEEE Xplore Digital Library) pp 1–4
- [25] Gear G W 1969 *Math. Comput.* **23** 119–25
- [26] Liu X, Strang G and Ott S 2003 *SIAM J. Discrete Math.* **16** 479–98
- [27] Beam R M and Warming R F 1993 *SIAM J. Sci. Comput.* **14** 971–1006
- [28] Boettcher A and Grudsky S M 2005 *Spectral Properties of Banded Toeplitz Matrices* (Philadelphia: SIAM) chapter 14
- [29] Golub G H and van Loan C F 1996 *Matrix Computations* (Baltimore, MD: The John Hopkins University Press)
- [30] Blow K J, Doran N J and Phoenix S J D 1992 *Opt. Commun.* **88** 137–40